2010

Robust isothermal electric control of exchange bias at room temperature

Xi He
University of Nebraska-Lincoln

Ning Wu
University of Nebraska-Lincoln

Anthony N. Caruso
University of Missouri-Kansas City, carusoan@umkc.edu

Elio Vescovo
Brookhaven National Laboratory, vescovo@bnl.gov

Kirill D. Belashchenko
University of Nebraska-Lincoln, belashchenko@unl.edu

See next page for additional authors

Authors
Xi He, Ning Wu, Anthony N. Caruso, Elio Vescovo, Kirill D. Belashchenko, Peter A. Dowben, and Christian Binek

nature materials

ARTICLES

PUBLISHED ONLINE: 20 JUNE 2010 | DOI: 10.1038/NMAT2785

Robust isothermal electric control of exchange bias at room temperature

Xi He[1], Yi Wang[1], Ning Wu[1], Anthony N. Caruso[2], Elio Vescovo[3], Kirill D. Belashchenko[1], Peter A. Dowben[1] and Christian Binek[1]*

Voltage-controlled spin electronics is crucial for continued progress in information technology. It aims at reduced power consumption, increased integration density and enhanced functionality where non-volatile memory is combined with high-speed logical processing. Promising spintronic device concepts use the electric control of interface and surface magnetization. From the combination of magnetometry, spin-polarized photoemission spectroscopy, symmetry arguments and first-principles calculations, we show that the (0001) surface of magnetoelectric Cr_2O_3 has a roughness-insensitive, electrically switchable magnetization. Using a ferromagnetic Pd/Co multilayer deposited on the (0001) surface of a Cr_2O_3 single crystal, we achieve reversible, room-temperature isothermal switching of the exchange-bias field between positive and negative values by reversing the electric field while maintaining a permanent magnetic field. This effect reflects the switching of the bulk antiferromagnetic domain state and the interface magnetization coupled to it. The switchable exchange bias sets in exactly at the bulk Néel temperature.

Spintronics strives to exploit the spin degree of freedom of electrons for an advanced generation of electronic devices[1,2]. In particular, voltage-controlled spin electronics is of vital importance to continue progress in information technology. The main objective of such an advanced technology is to reduce power consumption while enhancing processing speed, integration density and functionality in comparison with present-day complementary metal–oxide–semiconductor electronics[3–6]. Almost all existing and prototypical solid-state spintronic devices rely on tailored interface magnetism, enabling spin-selective transmission or scattering of electrons. Controlling magnetism at thin-film interfaces, preferably by purely electrical means, is a key challenge to better spintronics[7–10].

The absence of direct coupling between magnetization and electric field makes the electric control of collective magnetism in general, and surface and interface magnetism in particular, a scientific challenge. The significance of controlled interface magnetism started with the exchange-bias effect. Exchange bias is a coupling phenomenon at magnetic interfaces that manifests itself most prominently in the shift of the ferromagnetic hysteresis loop along the magnetic-field axis and is quantified by the magnitude $\mu_0 H_{EB}$ of the shift[11]. The exchange-bias pinning of ferromagnetic thin films is employed in giant magnetoresistance and tunnelling magnetoresistance structures of magnetic-field sensors and modern magnetic read heads[12].

Electric control of exchange bias has been proposed for various spintronic applications that go beyond giant magnetoresistance and tunnelling magnetoresistance technology[5]. One approach to such voltage control requires a reversible, laterally uniform, isothermal electric tuning of the exchange-bias field at room temperature, which remains a significant challenge.

Early attempts in electrically controlled exchange bias tried to exploit the linear magnetoelectric susceptibility of the antiferromagnetic material Cr_2O_3 as an active exchange-bias pinning system[13]. In a magnetoelectric material an applied electric field induces a net magnetic moment, which can be used to electrically manipulate the magnetic states of an adjacent exchange-coupled ferromagnetic film[14]. The small value of the maximum parallel magnetoelectric susceptibility $\alpha_{me}{}^{\parallel}(T = 263\,\mathrm{K}) \approx 4.13\,\mathrm{ps\,m^{-1}}$ of Cr_2O_3 (ref. 15) led many researchers to the conclusion that multiferroic materials are better suited for this purpose. Such materials have two or more ferroic order parameters, such as ferroelectric polarization and (anti)ferromagnetic order[16].

The potential for an increased magnetoelectric response, for the multiferroic materials, was dictated by the maximum possible value of $\alpha_{me}{}^{ij}$. It is determined by the geometric mean of the ferroic susceptibilities, both of which can individually be very high in multiferroics[17–20]. Coupling between these order parameters has been demonstrated[21]. However, it is typically weak, and the theoretical upper limit of $\alpha_{me}{}^{ij}$ is rarely reached[16].

Artificial two-phase multiferroics have been studied extensively. Such piezoelectric/ferromagnetic heterosystems allow for electric control of anisotropy[22,23]. However, strain-induced non-hysteretic magnetoelastic effects are often not stable (persistent) in the absence of an applied field (that is, volatile). Removing the electric field from a linear piezoelectric element releases the strain in the ferromagnetic component and hence restores the anisotropy of the piezoelectrically unstrained film. When using a ferroelectric material, to induce piezoelectric strain control, one may take advantage of the ferroelectric hysteresis to impose some residual strain that will persist after removing the electric field. In contrast to this electric control of magnetic anisotropy in two-phase multiferroics, we report on a non-volatile electric control of unidirectional magnetic anisotropy.

The most promising multiferroic single-phase materials used for electrically controlled exchange bias are $YMnO_3$ and $BiFeO_3$ (refs 24,25). Complete suppression of the exchange bias has been

[1]Department of Physics & Astronomy and the Nebraska Center for Materials and Nanoscience, University of Nebraska, Lincoln, Nebraska 68588-0111, USA, [2]Department of Physics, 257 Flarsheim Hall, University of Missouri, 5110 Rockhill Road, Kansas City, Kansas 64110, USA, [3]Brookhaven National Laboratory, National Synchrotron Light Source, Upton, New York 11973, USA. *e-mail: cbinek2@unl.edu.

achieved at 2 K in an $YMnO_3$/NiFe (permalloy) heterostructure. This effect, however, is irreversible. Moreover, the limitation of low temperatures makes $YMnO_3$ unsuitable for applications. The situation is better with $BiFeO_3$. In $BiFeO_3$/CoFe heterostructures, local magnetization reversal on a lateral length scale of up to 2 μm has been demonstrated[25,26]. However, global magnetization reversal, which could be revealed in macroscopic magnetic hysteresis, has not been achieved. Global, but not isothermal magnetoelectric switching has been achieved in the pioneering Cr_2O_3/CoPt heterostructure[13]. However, each sign reversal of the exchange-bias field required a new magnetoelectric annealing procedure, in which the pinning layer is cooled from $T > T_N$ to $T < T_N$ in the presence of both electric and magnetic fields. Isothermal electric control of exchange bias has been attempted by various groups, but with only marginal success[27,28]. The result was that reversible and global electrically controlled exchange bias carried out isothermally at room temperature remained elusive.

Here we reveal an unconventional ferromagnetism at the (0001) surface of the magnetoelectric antiferromagnet Cr_2O_3 and demonstrate its suitability for electrically controlled exchange bias and magnetization. New insights were achieved by combining first-principles calculations, general symmetry arguments, spin-resolved photoemission spectroscopy and magnetometry (see Supplementary Information) for the Cr_2O_3 (0001) surface and its interface in an exchange-bias heterostructure. We used a molecular beam epitaxy (MBE)-grown chromia thin film (see the Methods section) for the spin- and energy-resolved ultraviolet photoemission spectroscopy (UPS), whereas the isothermal electric control of exchange bias was done on a heterostructure involving an oriented chromia single crystal with (0001) surface. The choice of a high-quality single crystal for the exchange-bias system completely rules out sample heating induced by leakage currents because of the virtually perfect insulating properties of single-crystalline chromia. The UPS measurements have been carried out in zero electric field after magnetoelectric initialization of the antiferromagnetic domain state. The non-zero conductivity of thin films is a well-known experimental advantage used for the photoemission investigation of samples that otherwise are virtually perfectly insulating in the bulk. The finite conductivity of the thin film prevents charge accumulation, which could lead to misrepresented photoelectron energies.

On the basis of the understanding of the surface ferromagnetism of Cr_2O_3 (0001), a new concept of Cr_2O_3 (0001)-based exchange bias is implemented. As a result, a reversible, isothermal and global electric control of exchange bias is demonstrated at room temperature by reproducible electrically induced discrete shifts of the global magnetic hysteresis loop along the magnetic-field axis (see Supplementary Movie).

Magnetically uncompensated surfaces of antiferromagnetically ordered single crystals have been a subject of intense investigations, in particular in the framework of exchange bias[11]. The surface magnetization of an uncompensated antiferromagnetic surface with roughness usually averages out, so that only a small non-equilibrium statistical fluctuation remains for exchange coupling with the adjacent ferromagnet[29].

The surfaces of single-domain antiferromagnetic magnetoelectrics, such as the (0001) surface of the antiferromagnetically long-range ordered Cr_2O_3, are remarkable exceptions. The free energy of this system, with a boundary, depends on the polar vector **n** (external normal) as a macroscopic parameter. The existence of the magnetization at the boundary can be deduced from the reduction of the bulk magnetic point group by the presence of an invariant vector **n**. As both **n** and **E** are polar vectors, the boundary reduces the symmetry in a similar way to the electric field, **E**, in the bulk. An equilibrium magnetization must therefore exist at the surface of a magnetoelectric antiferromagnet, or at its interface with another material. This argument automatically includes equilibrium surface roughness; a more detailed analysis will be published elsewhere.

Both the bulk single crystal and the thin-film sample are confirmed to be (0001) oriented by X-ray diffraction. The surface topography of the bulk and the thin-film sample are mapped using atomic force microscopy (AFM). Figure 1 is organized in such a way that structural data of the bulk sample are shown in the upper panels of a and b. The corresponding data of the thin-film sample are shown in the lower panels of Fig. 1a,b. The (0001) orientation of the bulk surface is independently corroborated by the hexagonal reflection pattern obtained in low-energy electron diffraction. The prominent (0006) and (00012) X-ray peaks of the bulk sample are virtually identically reproduced in the thin film (compare peak positions in the upper and lower panels of Fig. 1a). The surface topography of the samples reveals a plateau with a root-mean-squared (r.m.s.) roughness of 0.88 nm for the surface of the bulk crystal (upper panel of Fig. 1b) and an even lower r.m.s. roughness of 0.19 nm (lower panel of Fig. 1b) for the thin-film sample measured along selected lines.

Figure 1c illustrates a configuration of the Cr_2O_3 (0001) surface. It is seen that the particular antiferromagnetic domain has an uncompensated surface magnetic monolayer with aligned moments on all surface Cr^{3+} ions, even if the surface is not atomically flat. Two features conspire to produce this property. First, the corundum lattice of Cr_2O_3 can be imagined as a layered arrangement of buckled Cr^{3+} ions sandwiched between the triangular layers of O^{2-} ions[30]. The electrostatically stable charge-neutral surface of this crystal is terminated by a semi-layer of Cr; this termination can be viewed as the cleavage of the crystal in the middle of the buckled Cr^{3+} layer[31]. Second, Cr ions, which are structurally similar with respect to the underlying O layer, have parallel spins. As a result, a single-domain antiferromagnetic state has all surface Cr spins pointing in the same direction. Note that although we have shown the surface Cr ions in bulk-like positions in Fig. 1, this assumption is immaterial for the existence of the surface magnetization, as follows from the general symmetry argument.

In single-crystalline Cr_2O_3, the antiferromagnetic order allows two degenerate 180° antiferromagnetic domains[14] (see Fig. 1 and Supplementary Fig. S1). These two domains have surface magnetizations of opposite sign. If the degeneracy of the two domain types is not lifted, the system develops a random multi-domain state with zero net surface magnetization when it is cooled below T_N. However, magnetoelectric annealing allows for preferential selection of one of these 180° domains by exploiting the free-energy gain $\Delta F = \alpha EH$ (ref. 14). As a result, even a rough Cr_2O_3 (0001) surface becomes spin-polarized when an antiferromagnetic single-domain state is established. Evidence of this roughness-insensitive surface magnetism is revealed by magnetometry (Supplementary Fig. S2 and Discussion) as well as spin-resolved UPS. Interpretation of the latter is supported by calculations of the site-resolved density of states (DOS) revealing a spin-polarized surface band above the valence-band maximum, in agreement with experimental findings. The UPS carried out on our MBE-grown Cr_2O_3 (0001) sample is sensitive to occupied surface electronic states.

Figure 2a shows the spin-polarized photoelectron intensity versus binding energy measured at 100 K. First, the MBE-grown Cr_2O_3 (0001) thin film has been cooled from $T > T_N$ in a small magnetic field of 30 mT alone, into a multidomain antiferromagnetic state. Spin-up and spin-down photoelectron intensities $I_{\uparrow,\downarrow}$ (red circles and blue squares) are virtually identical, indicating negligible net surface magnetization and polarization.

Furthermore, multiple measurements were undertaken for the single-antiferromagnetic-domain states, each with a fresh sample preparation. Subsequent sample preparations involve alternating

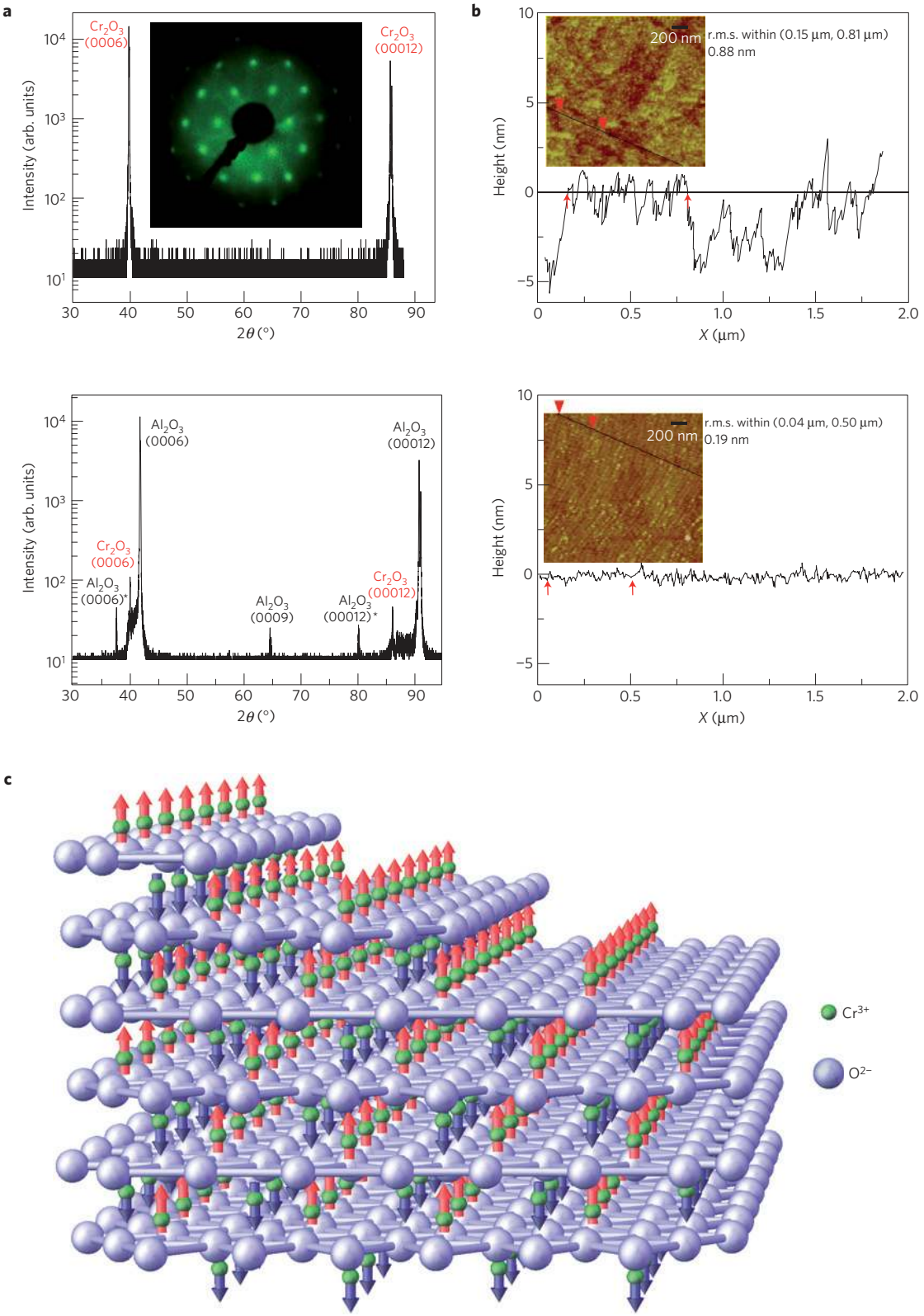

Figure 1 | Structural characterization. a, θ–2θ X-ray diffraction pattern of chromia bulk single crystal (upper panel) and thin film (lower panel) showing the chromia (0006) and (00012) peaks, respectively. The film is deposited on a sapphire (0001) substrate, giving rise to (0006), (00012), K_α and K_β (*) peaks and a weak structure-factor-forbidden (0009) peak. The inset shows a room-temperature low-energy electron diffraction pattern of the hexagonal chromia (0001) surface measured at an electron energy of 140 eV. **b**, Real-space topography of the chromia (0001) surface of bulk single crystal (upper panel) and thin film (lower panel) measured by AFM. The respective main frames show cross-sectional analysis along indicated lines. A r.m.s. roughness of 0.88 nm is calculated in the region between scanning position 0.15 and 0.81 μm for the bulk single crystal. The r.m.s. roughness of 0.19 nm of the thin film is measured between 0.04 and 0.50 μm. **c**, The spin structure of a Cr_2O_3 single crystal with a stepped (0001) surface is shown for one of its two antiferromagnetic single-domain states. Up (red) and down (dark blue) spins of the Cr^{3+} ions (green spheres) point along the *c* axis.

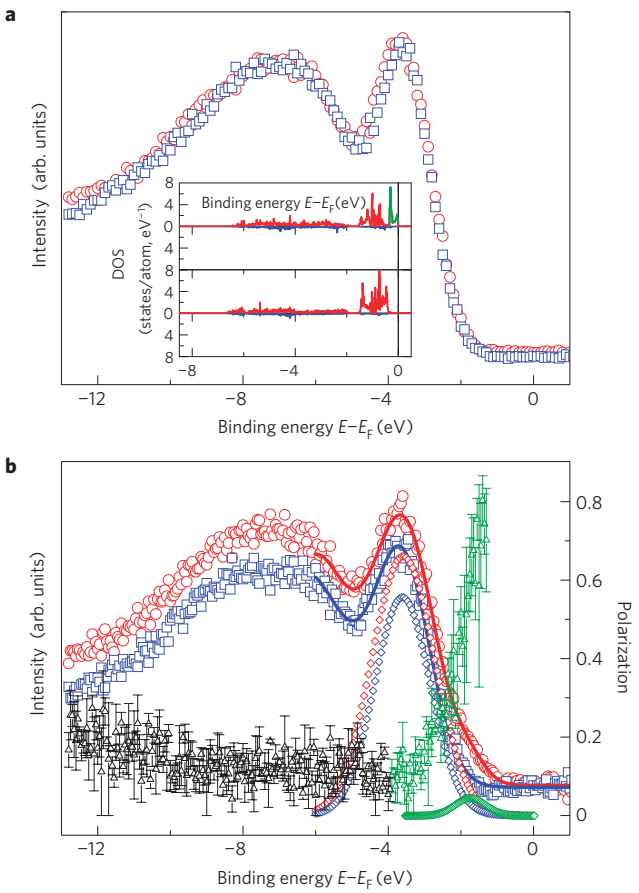

Figure 2 | Spin-polarized UPS measurements and layer-resolved DOS. **a**, The intensity of photoelectrons (occupied states) versus binding energy from a Cr_2O_3 (0001) surface measured at $T = 100$ K after cooling in $\mu_0 H = 30$ mT and $E = 0$ from $T > T_N$. Spin-up and spin-down intensities are shown by red circles and blues squares, respectively. Inset: The result of a first-principles calculation of the layer-resolved DOS. Colour code follows the experiment. The green line indicates a surplus surface state with spin-up polarization. **b**, Spin-up (red circles) and spin-down (blue squares) intensities after magnetoelectric annealing in $E = 3.85 \times 10^{-4}$ kV mm^{-1} and $\mu_0 H = 30$ mT. The lines are best fits of multiple-peak Gaussian functions. The diamonds show Cr 3*d* spin-up (red and green) and spin-down (blue) contributions extracted from the fits. The Gaussian fit shown by the green diamonds reflects specific surface states. Colour code matches the theoretical DOS data. The triangles show the contrast, *P*, in the spin-dependent intensities versus binding energy. The green triangles highlight the contribution from the surface state. Maximum absolute errors in *P* are indicated by bars.

magnetoelectric field cooling from above the Néel temperature to the target temperature of $T = 100$ K. The magnetoelectric annealing in alternating fields gives rise to alternating surface magnetization. This leads to a reproducible reversal of the spin-polarization measured at $T = 100$ K. Such data are then summed to provide an average overall net polarization, independent of instrumental asymmetry, as is the standard practice in spin-polarized photoemission and spin-polarized inverse photoemission.

The signal is clearly spin-split after magnetoelectric annealing in $E = 3.85 \times 10^{-4}$ kV mm^{-1} and $\mu_0 H = 30$ mT (compare red circles and blue squares in Fig. 2b), demonstrating high net spin-polarization at the surface. The spin contrast $P = (I_\uparrow - I_\downarrow)/(I_\uparrow + I_\downarrow)$, exhibited by triangles in Fig. 2b, is seen to increase significantly close to the valence-band maximum, E_F, (green triangles). We identify this feature with the contribution from the spin-polarized surface states of Cr 3*d* character. To corroborate this interpretation, we decompose the spin-dependent photoemission spectra $I_{\uparrow,\downarrow}$ into contributions from Cr 3*d* bulk and surface states. The contribution above the valence-band maximum (green) is interpreted as an extra spin-polarized surface state.

This interpretation is in accordance with our first-principles calculation of the layer-resolved DOS of the Cr_2O_3 (0001) surface shown in the inset of Fig. 2a. The DOS of a representative central layer with spin-up sublattice (majority/minority in red/blue) magnetization is shown by the lower two curves of the inset. The DOS of the surface layer is shown by the two upper curves in the inset of Fig. 2a. Note that in addition to the bulk states, a surplus spin-up density of states (green) appears above the valence-band maximum. This is consistent with our experimental findings in photoemission (Fig. 2b) and magnetometry (Supplementary Fig. S2 and Discussion).

Experimental and theoretical evidence together point very strongly to the existence of a roughness-insensitive ferromagnetic state at the Cr_2O_3 (0001) surface when the underlying Cr_2O_3 single crystal is in an antiferromagnetic single-domain state. Our findings indicate that the surface has a magnetization and is spin-polarized, despite the roughness that is evidently present according to our AFM investigations. Although the roughness may have some effect on the magnitude of the surface magnetization, its mere presence is unusual, and further supported by the experiments on electrically switched exchange bias.

The ferromagnetic surface moment can be isothermally switched by electrical means, giving rise to reversible switching of large exchange-bias fields in our perpendicular exchange-bias heterostructure Cr_2O_3(0001)/Pd 0.5 nm/(Co 0.6 nm Pd 1.0 nm)$_3$. The Cr_2O_3 substrate in the exchange-bias heterostructure is a (0001) bulk single crystal. The temperature dependence of the exchange bias and its relation to the temperature dependence of the chromia surface magnetization are discussed in the Supplementary Discussion.

Figure 3 demonstrates large isothermal electric switching of the exchange-bias field. It is achieved by leaving the realm of the linear magnetoelectric effect, which gives rise to only a minuscule electric control effect[27,28]. In contrast to this small linear effect, significant electrically controlled switching requires that a critical threshold given by the product $|EH|_c$, where E and H are isothermally applied axial electric and magnetic fields, is overcome. Initially the heterostructure has been magnetoelectrically annealed in $EH > 0$ with $E = 0.1$ kV mm^{-1} and $\mu_0 H = 77.8$ mT down to $T = 303$ K. The hysteresis loops are measured isothermally at $T = 303$ K and $E = 0$. The red squares in Fig. 3a,b show the same virgin loop with positive exchange bias of $\mu_0 H_{EB} = +6$ mT. Next, without changing the temperature, a field product $EH < 0$ of individual fields $E = -2.6$ kV mm^{-1} and $\mu_0 H = +154$ mT is applied for less than a second. During the time when an electric field is applied, the electric current is monitored to stay below 0.01 μA, resulting in virtually zero sample heating. After applying the electric- and magnetic-field product a magnetic hysteresis loop is measured in $E = 0$. Green triangles (Fig. 3a) show the resulting loop with a pronounced negative exchange bias of $\mu_0 H_{EB} \approx -13$ mT. The same field product is achieved with $E = +2.6$ kV mm^{-1} and $\mu_0 H = -154$ mT, having the same effect on the exchange bias as shown in Fig. 3b by blue circles. The isothermal switching of the exchange-bias field implies a field-induced switching of the antiferromagnetic single-domain state of Cr_2O_3 into the opposite antiferromagnetic registration. This switching is accompanied by a reversal of the interface magnetization. Figure 3c shows a sequence of switched exchange-bias fields obtained by switching the electric field back and forth between $E = +2.6$ kV mm^{-1} and $E = -2.0$ kV mm^{-1} at constant set field $\mu_0 H = -154$ mT, all at a constant temperature $T = 303$ K. The reproducible switching shows no signs of ageing. The asymmetry between positive and negative

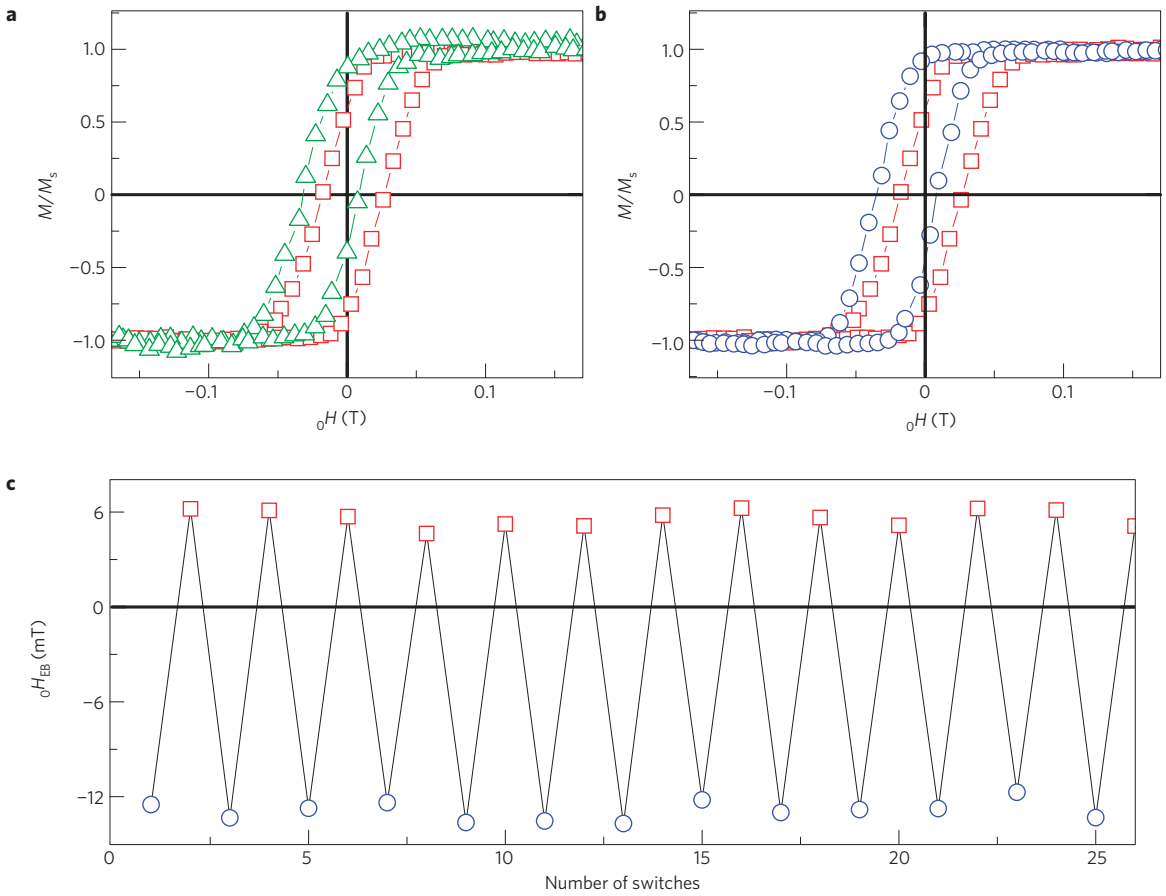

Figure 3 | Isothermal electric switching of the exchange-bias field. a, Exchange-biased hysteresis loops of Cr_2O_3 (0001)/Pd 0.5 nm/(Co 0.6 nm Pd 1.0 nm)$_3$ at $T = 303$ K after initial magnetoelectric annealing in $E = 0.1$ kV mm^{-1} and $\mu_0 H = 77.8$ mT. Hysteresis loops are measured by polar Kerr magnetometry in $E = 0$, respectively. The red squares show the virgin curve with a positive exchange-bias field of $\mu_0 H_{EB} = +6$ mT. Isothermal-field exposure in $E = -2.6$ kV mm^{-1} and $\mu_0 H = +154$ mT gives rise to a loop with a negative exchange-bias field of $\mu_0 H_{EB} \approx -13$ mT (green triangles). **b**, The red squares show the same virgin reference loop. The blue circles show the hysteresis loop after isothermal-field exposure in $E = +2.6$ kV mm^{-1} and $\mu_0 H = -154$ mT, giving rise to the same negative exchange bias of $\mu_0 H_{EB} = -13$ mT. **c**, $\mu_0 H_{EB}$ versus number of repeated isothermal switching through exposure to $E = +2.6$ kV mm^{-1} (blue circles) and $E = -2$ kV mm^{-1} (red squares) at constant $\mu_0 H = -154$ mT, respectively.

exchange-bias values is a consequence of a difference in the interface magnetization $S_{Cr_2O_3}$ for negative and positive exchange bias.

A nonlinear magnetoelectric switching of the antiferromagnetic single-domain state of Cr_2O_3 was reported as far back as 1966 by Martin and Anderson[32]. Their work illustrated that the isothermal switching between the two different antiferromagnetic domains of Cr_2O_3 is possible if sufficiently strong field products $E \cdot H$ are applied along the c axis[32]. This switching is a thermally activated process. At constant temperature there is a critical value $|EH|_c$, above which the system settles into the single-domain state with the lowest free energy, even if this requires a switching of the entire antiferromagnetic spin structure. This hysteretic switching of Cr_2O_3 is directly reflected in the hysteresis of the electric-field dependence of the exchange-bias field.

Figure 4 shows the threshold character of electric switching at $T = 303$ K. All data are taken after magnetoelectric annealing in $E = 0.1$ kV mm^{-1} and $\mu_0 H = 77.8$ mT. The hysteretic electric-field dependence, $\mu_0 H_{EB}$ versus E, is determined from individual magnetic hysteresis loops measured in $E = 0$. Each data point results from a loop measured after isothermal exposure of the sample to one of various E-fields and fixed magnetic field $\mu_0 H = -115$ mT (circles), $\mu_0 H = -154$ mT (triangles) and $\mu_0 H = -229$ mT (squares), respectively. Note that the same values of the field products can be achieved for various corresponding positive magnetic fields $\mu_0 H = +115, +154$ and $+229$ mT. The resulting electrically controlled switching is shown in Supplementary Fig. S4. Two main characteristics are observed in the $\mu_0 H_{EB}$ versus E data. First, for a given positive magnetic field there is a critical negative and positive electric field, E_c, where switching of the exchange-bias field takes place. The rectangular hysteresis $\mu_0 H_{EB}$ versus E is in perfect agreement with the isothermal switching of the antiferromagnetic domain state of Cr_2O_3 reported in ref. 32. This includes details such as the asymmetry between the negative and the positive switching field.

The insets of Fig. 4 show that the critical switching fields of the exchange bias obey the relation $|EH|_c = \text{const}$ corresponding to the switching of the Cr_2O_3 antiferromagnetic single domain[32]. Solid squares are data points of E_c for magnetic fields $\mu_0 H = -115, -154$ and -229 mT. The lines are fits of the functional form $H = \text{const}/E_c$. This shows that the switching effect originates from the coherent flip of the antiferromagnetic registration of the Cr_2O_3 pinning system. The inversion of the antiferromagnetic spin structure is accompanied by the reversal of the Cr_2O_3 (0001) interface magnetization, which in turn causes switching of the exchange-bias field. As this switching is induced at a threshold of the product $|EH|_c$, the H-field can be made arbitrarily small when E is scaled up accordingly. There is plenty of room for E-field increase by shrinking the thickness of the pinning layer down to the nanoscale. It is feasible to use nanostructured arrays of permanent magnetic nanopillars to apply magnetic stray

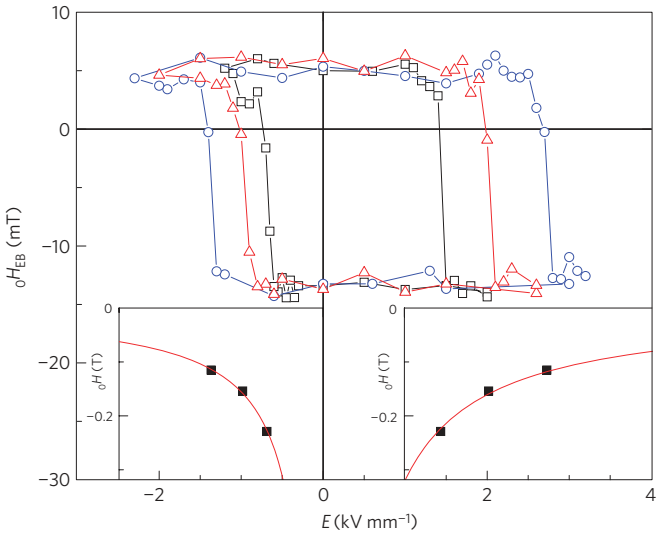

Figure 4 | Hysteretic electric-field dependence of the exchange-bias field. $\mu_0 H_{EB}$ versus E, measured at $T = 303$ K from individual Kerr loops. Data are taken after initial magnetoelectric annealing of Cr_2O_3 (0001)/Pd 0.5 nm/(Co 0.6 nm Pd 1.0 nm)$_3$ in axial fields $E = 0.1$ kV mm^{-1} and $\mu_0 H = 77.8$ mT. Kerr loops are measured in $E = 0$ after isothermal E-field and simultaneous H-field exposure of the sample. For a given $\mu_0 H_{EB}$ versus E curve the magnetic field is constant. The three $\mu_0 H_{EB}$ versus E data sets correspond to $\mu_0 H = -115$ mT (circles), $\mu_0 H = -154$ mT (triangles) and $\mu_0 H = -229$ mT (squares), respectively. The solid squares in the insets show the data points of electric switching fields and corresponding magnetic fields $\mu_0 H = -115, -154$ and -229 mT. The lines are single-parameter fits of the functional form $H = \text{const}/E_c$.

fields below the coercive field of the CoPd film. For instance, the field 20 nm from the end of a Ni rod, 175 nm long and 20 nm diameter, has been estimated as ~25 mT (ref. 33). The insets of Fig. 4 show that a magnetic stray field of 20 mT requires a maximum electric switching field of 16 kV mm^{-1} to reverse the exchange-bias field and ferromagnetic magnetization. Chromia is known for its excellent dielectric properties, and is used as a good insulator with high dielectric breakdown fields of 10^7 V cm^{-1} = 1,000 kV mm^{-1} at room temperature. Still it will remain a challenge to achieve these dielectric properties in thin films.

Electric control of magnetism, at room temperature, is the basis of advanced spintronics for post-metal–oxide–semiconductor technology. The intensive research efforts on multiferroic materials of recent years are to a large extent driven by the possibilities of electrically controlled magnetism at room temperature. We have shown by a combination of experiment and theory that Cr_2O_3, the archetypical magnetoelectric antiferromagnet, is revived as a candidate for reversible electric control of magnetism at room temperature. This control is made possible by the roughness-insensitive ferromagnetic spin state at the (0001) surface of Cr_2O_3. In the highly nonlinear magnetoelectric regime the antiferromagnetic order can be electrically switched along with the surface magnetization. This phenomenon takes place at the interface between Cr_2O_3 (0001) and a ferromagnetic Co/Pd multilayer film. In this perpendicular exchange-bias system, a reversible and global electric switching of the exchange-bias field was realized isothermally at room temperature. This observation opens up exciting prospects for spintronics applications.

Methods

MBE is used for the sample growth. *Ex situ* structural characterization is done by X-ray diffraction techniques. The magnetic characterization is primarily based on the polar magneto–optical Kerr effect and partially carried out with the help of a superconducting quantum interference device. The Cr_2O_3 (0001) surface of the c−Al_2O_3/Cr(110)[8 nm]/Cr_2O_3(0001)[103 nm] sample was cleaned by ion-beam sputtering and post-sputtering annealing procedures before the photoemission measurements. Spin-polarized angle-resolved photoemission spectra were acquired at the U5UA undulator spherical grating monochromator beamline at the National Synchrotron Light Source. The electronic structure calculations of the Cr_2O_3 (0001) surface were carried out using the projected augmented wave method as implemented in the Vienna *ab initio* simulation program[34–36].

Received 30 December 2009; accepted 18 May 2010; published online 20 June 2010

References

1. Wolf, S. A. *et al.* Spintronics: A spin-based electronics vision for the future. *Science* **294,** 1488–1495 (2001).
2. Žutić, I., Fabian, J. & Das Sarma, S. Spintronics: Fundamentals and applications. *Rev. Mod. Phys.* **76,** 323–410 (2004).
3. Zhirnov, V. V., Hutchby, J. A., Bourianoff, G. I. & Brewer, J. E. Emerging research logic devices. *IEEE Circuits Devices* **21,** 37–46 (2005).
4. Ney, A., Pampuch, C., Koch, R. & Ploog, K. H. Programmable computing with a single magnetoresistive element. *Nature* **425,** 485–487 (2003).
5. Binek, Ch. & Doudin, B. Magnetoelectronics with magnetoelectrics. *J. Phys. Condens. Matter* **17,** L39–L44 (2005).
6. Dery, H., Dalal, P., Cywiński, Ł. & Sham, L. J. Spin-based logic in semiconductors for reconfigurable large-scale circuits. *Nature* **447,** 573–576 (2007).
7. Zavaliche, F. *et al.* Electrically assisted magnetic recording in multiferroic nanostructures. *Nano Lett.* **7,** 1586–1590 (2007).
8. Tsymbal, E. Y. & Kohlstedt, H. Applied physics: Tunneling across a ferroelectric. *Science* **313,** 181–183 (2006).
9. Maruyama, T. *et al.* Large voltage-induced magnetic anisotropy change in a few atomic layers of iron. *Nature Nanotech.* **4,** 158–161 (2008).
10. Velev, J. P., Dowben, P. A., Tsymbal, E. Y., Jenkins, S. J. & Caruso, A. N. Interface effects in spin-polarized metal/insulator layered structures. *Surf. Sci. Rep.* **63,** 400–425 (2008).
11. Nogués, J. & Schuller, I. K. Exchange bias. *J. Magn. Magn. Mater.* **192,** 203–232 (1999).
12. Chappert, C., Fert, A. & Van Dau, F. N. The emergence of spin electronics in data storage. *Nature Mater.* **6,** 813–823 (2007).
13. Borisov, P., Hochstrat, A., Chen, X., Kleemann, W. & Binek, Ch. Magnetoelectric switching of exchange bias. *Phys. Rev. Lett.* **94,** 117203 (2005).
14. O'Dell, T. H. *The Electrodynamics of Magneto–Electric Media* (North-Holland, 1970).
15. Borisov, P., Hochstrat, A., Shvartsman, V. V. & Kleemann, W. Superconducting quantum interference device setup for magnetoelectric measurements. *Rev. Sci. Instrum.* **78,** 106105 (2007).
16. Fiebig, M. Revival of the magnetoelectric effect. *J. Phys. D* **38,** R123–R152 (2005).
17. Wang, J. *et al.* Epitaxial $BiFeO_3$ multiferroic thin film heterostructures. *Science* **299,** 1719–1722 (2003).
18. Hur, N. *et al.* Electric polarization reversal and memory in a multiferroic material induced by magnetic fields. *Nature* **429,** 392–395 (2004).
19. Eerenstein, W., Mathur, N. D. & Scott, J. F. Multiferroic and magnetoelectric materials. *Nature* **442,** 759–765 (2006).
20. Bibes, M. & Barthélémy, A. Multiferroics: Towards a magnetoelectric memory. *Nature Mater.* **7,** 425–426 (2008).
21. Lottermoser, T. *et al.* Magnetic phase control by an electric field. *Nature* **430,** 541–544 (2004).
22. Sahoo, S. *et al.* Ferroelectric control of magnetism in $BaTiO_3$/Fe heterostructures via interface strain coupling. *Phys. Rev. B* **76,** 092108 (2007).
23. Weiler, M. *et al.* Voltage controlled inversion of magnetic anisotropy in a ferromagnetic thin film at room temperature. *New J. Phys.* **11,** 013021 (2009).
24. Laukhin, V. *et al.* Electric-field control of exchange bias in multiferroic epitaxial heterostructures. *Phys. Rev. Lett.* **97,** 227201 (2006).
25. Chu, Y-H. *et al.* Electric-field control of local ferromagnetism using a magnetoelectric multiferroic. *Nature Mater.* **7,** 478–482 (2008).
26. Zhao, T. *et al.* Electrical control of antiferromagnetic domains in multiferroic $BiFeO_3$ films at room temperature. *Nature Mater.* **5,** 823–829 (2006).
27. Liu, J. P., Fullerton, E., Gutfleisch, O. & Sellmyer, D. J. (eds) in *Nanoscale Magnetic Materials and Applications* Ch. 6 (Springer, 2009).
28. Lim, S-H. *et al.* Exchange bias in thin-film $(Co/Pt)_3/Cr_2O_3$ multilayers. *J. Magn. Magn. Mater.* **321,** 1955–1958 (2009).
29. Kuch, W. *et al.* Tuning the magnetic coupling across ultrathin antiferromagnetic films by controlling atomic-scale roughness. *Nature Mater.* **5,** 128–133 (2006).
30. Krichevtsov, B. B., Pavlov, V. V. & Pisarev, R. V. Nonreciprocal optical effects in antiferromagnetic Cr_2O_3 subjected to electric and magnetic fields. *Zh. Eksp. Teor. Fiz.* **94,** 284–295 (1988).

31. Freund, H-J., Kuhlenbeck, H. & Staemmler, V. Oxide surfaces. *Rep. Prog. Phys.* **59,** 283–347 (1996).
32. Martin, T. J. & Anderson, J. C. Antiferromagnetic domain switching in Cr_2O_3. *IEEE Trans. Magn.* **2,** 446–449 (1966).
33. Bromwich, T. J. *et al.* Remanent magnetic states and interactions in nano-pillars. *Nanotechnology* **17,** 4367–4373 (2006).
34. Kresse, G. & Hafner, J. *Ab initio* molecular dynamics for open-shell transition metals. *Phys. Rev. B* **48,** 13115–13118 (1993).
35. Kresse, G. & Furthmueller, J. Efficiency of *ab inito* energy calculations for metals and semiconductors using a plane-wave basis set. *Comput. Mater. Sci.* **6,** 15–50 (1996).
36. Kresse, G. & Furthmueller, J. Efficient iterative schemes for *ab initio* total-energy calculations using a plane-wave basis set. *Phys. Rev. B* **54,** 11169–11186 (1996).

Acknowledgements

This work is supported by NSF through Career DMR-0547887, by the Nebraska Research Initiative (NRI), by the NSF MRSEC Grant No. 0820521 and by the NRC/NRI supplement to MRSEC. K.D.B. is a Cottrell Scholar of Research Corporation. Technical help from S-Q. Shi, V. R. Shah and L. P. Yue in the calculation of DOS, taking XRD and AFM data is acknowledged, respectively. We are thankful to Crystal GmbH for providing excellent Cr_2O_3 single crystals.

Author contributions

X.H. and C.B. designed the study, in particular conceiving the electrically controlled exchange bias and electrically controlled magnetism. Y.W. and X.H. collected and analysed the magnetic data. N.W. led the photoemission experiments and data analysis. A.C. and E.V. supported the photoemission experiments. K.D.B. conceived the concept of roughness-insensitive surface magnetization and directed the electronic structure calculations. P.A.D. directed and conceived the photoemission experiments. C.B. directed the overall study. All authors contributed to the scientific process and the refinement of the manuscript. C.B. and X.H. wrote most of the paper.

Additional information

The authors declare no competing financial interests. Supplementary information accompanies this paper on www.nature.com/naturematerials. Reprints and permissions information is available online at http://npg.nature.com/reprintsandpermissions. Correspondence and requests for materials should be addressed to C.B.

nature materials

SUPPLEMENTARY INFORMATION

DOI: 10.1038/NMAT2785

Robust isothermal electric control of exchange bias at room temperature

Xi He[1], Yi Wang[1], Ning Wu[1], Anthony N. Caruso[2], Elio Vescovo[3], Kirill D. Belashchenko[1], Peter A. Dowben[1], Christian Binek[1,*]

[1]*Department of Physics & Astronomy and the Nebraska Center for Materials and Nanoscience, University of Nebraska, Lincoln, NE, 68588-0111, USA*

[2]*Department of Physics, 257 Flarsheim Hall, University of Missouri, 5110 Rockhill Road, Kansas City KS 64110, USA*

[3]*Brookhaven National Laboratory, National Synchrotron Light Source, Upton, NY, 11973, USA*

[*]To whom correspondence should be addressed. E-mail: cbinek2@unl.edu

DOI: 10.1038/NMAT2785

1. Supplementary Figures and Legends

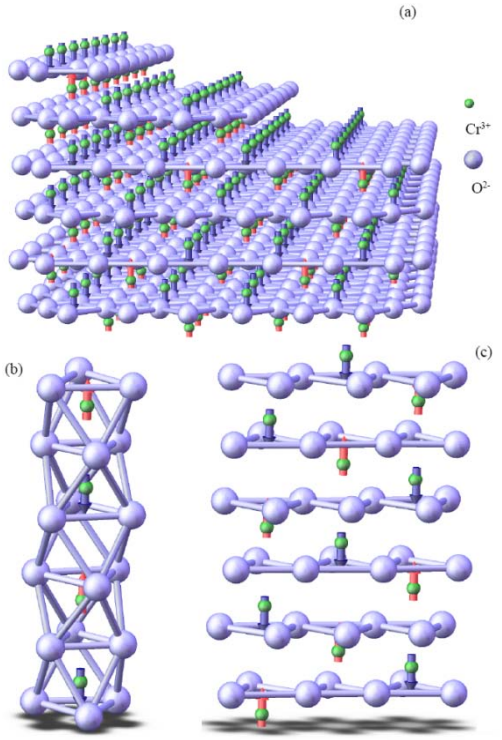

Supplementary Fig. 1: (a) Spin structure of a Cr_2O_3 single crystal with a stepped (0001) surface is shown for one of its two AF single domain states inverted with respect to Fig.1. Up (red) and down (dark blue) spins of the Cr^{3+} ions (green spheres) point along the *c*-axis. (b) Light blue spheres represent the O^{2-} ions which are arranged in chains of face-sharing distorted octahedra surrounding the Cr^{3+} ions. (c) Shows a more detailed view of the buckled arrangement of the Cr^{3+} ions sandwiched between adjacent oxygen layers.

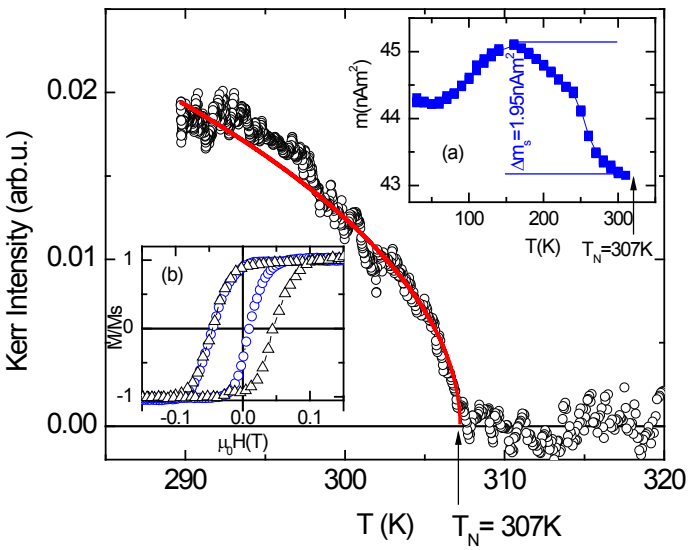

Supplementary Fig. 2: Temperature dependence of the polar Kerr signal (circles) of (0001)Cr_2O_3(15nm)/Cr(5nm). The Néel temperature T_N=307K with the onset of Kerr intensity is indicated by an arrow. The line shows a $\sqrt{T_N - T}$ -fit of the Kerr data. Inset (a) depicts the *T*-dependence of the axial magnetic moment, *m*, of the sample in an applied axial field of $\mu_0 H$ = 0.05T. Horizontal lines indicate the maximum change in *m* vs. *T*.

Inset (b) shows the magnetic hysteresis loops of the Cr_2O_3(0001)/CoPd exchange bias heterostructure (circles) and the Al_2O_3(0001)/CoPd reference sample both measured with the help of polar Kerr magnetometry at T = 296 K after field cooling from $T > T_N$ in an axial field of $\mu_0 H$ = 0.3 T. The exchange bias loop shift of $\mu_0 H_{EB}$=-16.7 mT is indicated by an arrow.

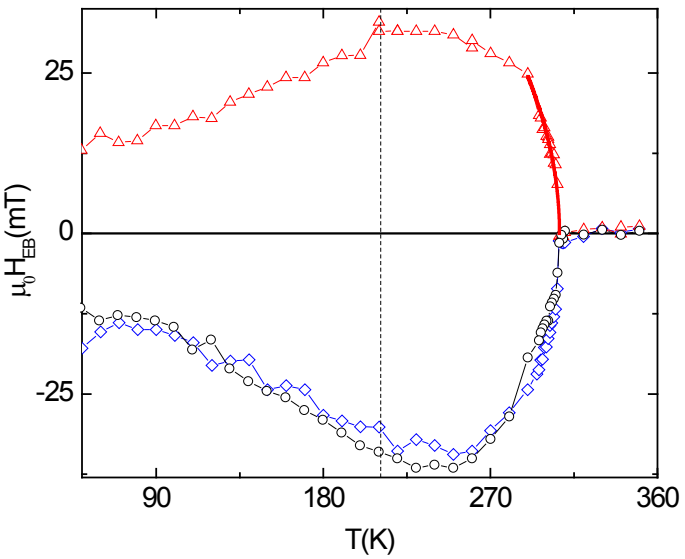

Supplementary Fig. 3: Temperature dependence of the exchange bias field, $\mu_0 H_{EB}$ vs. T, measured after magnetic field cooling (circles) and magnetoelectric annealing in E= ± 1620 kV/m electric and $\mu_0 H$= 0.3 T magnetic field (diamonds E<0, triangles E>0) for increasing temperature, respectively. The solid line is the result of a $\sqrt{T_N - T}$ -fit of $\mu_0 H_{EB}$ vs. T data (circles) at 290K<T<307K.

DOI: 10.1038/NMAT2785

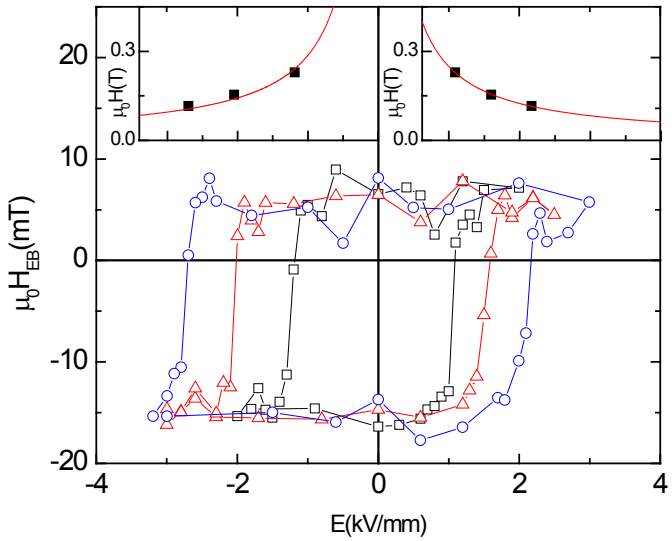

Supplementary Fig. 4: Hysteretic electric field dependence of the exchange bias field, $\mu_0 H_{EB}$ vs. E, measured at T = 303 K from individual Kerr loops. Data are taken after initial magnetoelectric annealing of Cr_2O_3 (0001)/Pd0.5nm/(Co0.6nmPd1.0nm)$_3$ in axial fields E = 0.1 kV/mm and $\mu_0 H = 77.8$ mT. Kerr loops are measured in E = 0 after isothermal E-field and simultaneous H-field exposure of the sample. For a given $\mu_0 H_{EB}$ vs. E curve the magnetic field is constant. The three $\mu_0 H_{EB}$ vs. E data sets correspond to $\mu_0 H = +115$ mT (circles), $\mu_0 H = +154$ mT (triangles), and $\mu_0 H = +229$ mT (squares), respectively. The solid squares in the insets (a) and (b) show the data points of electric switching fields and corresponding magnetic fields $\mu_0 H = +115$, +154 and +229 mT. The lines are single parameter fits of the functional form $H = \text{const} / E_c$.

2. Supplementary Methods

The sample investigated in our electrically controlled exchange bias experiments has been grown by molecular beam epitaxy (MBE) at a base pressure of 1.3×10^{-10} mbar which increases to 5×10^{-10} mbar during growth. A commercial Cr_2O_3 single crystal (Crystal GmbH) with an optically flat (0001) surface has been heated to T = 723 K and maintained under ultra high vacuum (UHV) condition for 3 hours. Next a Pd[0.5nm]/(Co[0.6nm]Pd[1.0nm])$_3$ multilayer with perpendicular magnetic anisotropy has been MBE grown keeping the Cr_2O_3 substrate at T = 473 K. Growth rates of 0.87 nm/min and 0.31 nm/min for Pd and Co, respectively have been monitored using a quartz resonator. A reference FM thin film has been deposited by identical means on a diamagnetic sapphire (0001) substrate. A Cr_2O_3 (0001) thin film used for spin-resolved photo-emission and magneto-optical Kerr effect has been grown by MBE. A Cr (110) seed layer of 8nm thickness has been deposited on the *c*-plane of a sapphire single crystal kept at T=573 K during growth. Subsequently the (0001) Cr_2O_3 film has been grown on top of the seed layer by Cr evaporation in the presence of molecular oxygen gas at a

partial pressure of 2.6×10^{-6} mbar and substrate temperature of T=573 K. The growth procedure described above results in the final structure c-Al_2O_3/Cr (110)[8nm]/Cr_2O_3 (0001)[103nm]. Ex-situ small and wide angle X-ray diffraction has been used for structural analysis of the various samples. A second thin film sample grown by MBE under identical conditions with an additional Cr top electrode of 6 nm thickness has been used for the SQUID measurement. The SQUID measurements with this sample provide independent support that the surface moment of the chromia (0001) surface is maintained at an interface with a metal.

The magnetic characterization was done primarily with the help of polar magneto-optical Kerr effect. Magnetic and electric fields are applied normal to the sample surface. The polarized incident laser beam of wavelength λ=670 nm is reflected from the sample surface in normal incidence geometry. Glan-Thompson polarizers are used for polarizing and analyzing of the light. The reflected beam is periodically modulated between left and right circularly polarized light by the photo-elastic modulator (PEM). Modulation takes place with a frequency of 50 kHz and a phase amplitude of $\varphi_0 = 175^0$ which maximizes the Bessel-function $J_2(\varphi)$. The modulation signal is used as reference signal for a lock-in amplifier. The orthogonal retarder axes of the PEM are perpendicular and parallel aligned to the plane of incidence, respectively. The subsequent analyzer makes an angle of 45^0 to the retarder axes. The transmitted intensity modulated light is detected by a photodiode providing the input signal to the lock-in amplifier. Its second harmonic Fourier component is proportional to the off-diagonal Fresnel reflection coefficient r_{sp} and, hence, proportional to the magnetization of the sample within the penetration depth of the light beam. In addition a superconducting quantum interference device (Quantum-Design MPMS XL-7) has been used for measurements of the absolute magnetic moment of the Cr_2O_3 (0001) sample and its surface in particular.

The Cr_2O_3(0001) surface of the c-Al_2O_3/Cr(110)[8 nm]/Cr_2O_3(0001) [103 nm] sample was cleaned by ion-beam sputtering and post-sputtering annealing procedures prior to the photoemission measurements. Spin polarized angle resolved photoemission spectra were acquired at the U5UA undulator spherical grating monochromator (SGM) beamline at the National Synchrotron Light Source (NSLS)[37, 38, 39]. Linearly polarized light from an undulator source was monochromatized using a spherical grating monochromator (SGM) and the ultra-high-vacuum photoemission end station was equipped with a commercial angle-resolved hemispherical electron energy analyzer (EA125, Omicron GmbH) and a post electron energy analyzer Mott detector for spin polarization analysis[37, 38, 39]. The spin polarization P for the collected data was determined according to

$$P = \frac{1}{2}\frac{\sqrt{I_L^+ I_R^-} - \sqrt{I_L^+ I_R^-}}{\sqrt{I_L^+ I_R^-} + \sqrt{I_L^+ I_R^-}},$$

where I_L and I_R represent the number of electrons scattered into the left and right channels of the Mott detector, respectively. The spin-resolved photoemission spectra were measured repeatedly at T=100 K with at an incident photon energy of $h\nu = 58.2$ eV and combined energy resolution of $\Delta E = 120$ meV. Measurements of energy and spin-resolved photoemission can be perturbed by magnetic stray fields. Hence, a magnetoelectric annealing procedure was performed prior to the spin-polarized photoemission measurements using a small applied magnetic and a simultaneously applied electric field is crucial for establishing the antiferromagnetic single domain state.

DOI: 10.1038/NMAT2785

Next we describe the decomposition of the photo-emission intensity into Cr and oxygen bulk and surface contributions. The lines in Fig. 2b are results of best fits based on superimposed Gaussian functions. The fits represent the sum of Cr and oxygen contributions to spin up (red) and spin down (blue) intensities. The diamonds in Fig. 2b show the sole Cr contributions as obtained from the fits. The spin down states (blue) can be fitted by a single Gaussian function. Remarkably, the best fit of the spin up intensity requires two Gaussian functions (red and green).

Detailed structural characterization of the chromia sample has been performed by θ-2θ wide angle X-ray diffraction (XRD) and using the Cu-K_α source of a Bruker-AXS D8 diffractometer.

Prior to the low energy electron diffraction experiment the chromia (0001) has been treated by an ion sputtering and annealing procedure identical to the preparation for the photoemission experiment. The LEED pattern has been recorded under UHV condition at room temperature using monoenergetic electrons of 140 eV kinetic energy and prepared in the same manner as the samples for spin polarized photoemission.

A Digital Instruments EnviroScope Atomic Force Microscope has been used for a topography scan in a 2μm×2μm region. The software package of this instrument has been used for section analysis and corresponding calculation of root mean square roughness.

The electronic structure calculations of the Cr_2O_3 (0001) surface were performed using the projected augmented wave (PAW) method[40] as implemented in the *ab initio* total energy and molecular dynamics program VASP (Vienna *ab initio* simulation program)[41,42,43,44]. The electron-electron interaction is described using the spherically-symmetric version of the LSDA+U method with the parameters $U = 4.0$ eV and $J = 0.58$ eV for the Cr 3*d* electrons, which provide excellent description of the bulk properties of Cr_2O_3[45,46]. The (0001) surface is modeled by a symmetric slab containing eight O layers, 7 bulk-like buckled Cr layers, and a semi-layer of Cr on each surface of the slab. The terminating Cr atoms are placed in the bulk-like positions, which were found to be energetically favorable. The atomic positions were fully optimized while keeping the in-plane lattice translations fixed at their calculated bulk values; the Hellman-Feynman forces were converged to less than 0.01 eV/Å. This optimization and electronic self-consistency were performed using the plane-wave cutoff of 520 eV and a 4×4×1 Monkhorst-Pack *k*-point mes[47] with a 0.2 eV Gaussian smearing. The site-resolved densities of states were then calculated using a 8×8×1 *k*-point mesh and the modified tetrahedron method[48]. Further details on the surface structure, energetics, and magnetism will be reported in a forthcoming theoretical publication.

3. Supplementary discussion

Supplementary Fig. 2 shows the temperature dependence of the local magneto-optical Kerr signal measured in polar reflection geometry in zero applied field on a 15nm Cr_2O_3 (0001) thin film. The latter is covered with a protective Cr thin film of 5nm thickness. The incoming laser beam is probing a spot with a lateral size of about 19.6 mm^2. The Kerr signal reveals a residual FM moment with a temperature dependence roughly following the power law behavior of a classical order-parameter (line). The onset of a polar Kerr signal at $T < T_N = 307$K indicates a gradually increasing local imbalance between up and down FM surface domains within the finite area probed by the laser spot. The positive or negative surface magnetization of each domain originates from the

surface spin structure of the AF bulk domains. The smallness and, hence, high noise level of the signal reflects the fact that most of the spontaneous surface magnetization mutually cancels out in a multi domain state. Magnetoelectric annealing of a Cr_2O_3 single crystal allows producing a single domain state and a laterally uniform Kerr signal can be measured across the (0001) surface. [49] They discussed their early experimental findings phenomenologically in terms of non-reciprocal light reflection using general symmetry arguments without reference to the intuitive microscopic explanation of a FM surface state evidenced here. However, the remarkable similarity of the temperature behavior of the Kerr signal measured from Cr_2O_3 (0001)/vacuum[49] and a Cr-covered Cr_2O_3 (0001) surface (supplementary Fig. 2) implies that the surface magnetic state survives as interface magnetization in bilayer systems, as required by symmetry. This detail is significant for our Cr_2O_3 (0001)-based exchange bias system.

The FM surface state is further evidenced by quantitative measurements of the axial magnetization of a 200nm Cr_2O_3 (0001) thin film covered with a 5nm Pt electrode using superconducting quantum interference magnetometry. The inset (a) of supplementary Fig. 2 displays the temperature dependence of the magnetic moment, m, for an axial magnetic field of $\mu_0 H$ = 0.05T applied along the c-axis. The change in the magnetic moment between the background value at $T = T_N$ and the maximum value at about T = 260K is $\Delta m = 1.95\times10^{-9}$ Am^2 (see inset (a) supplementary Fig.2). A straightforward estimate suggests that Δm originates from a fully polarized surface layer of Cr^{3+} magnetic moments. With a sample surface of $A = 25\times10^{-6}$ m^2 and 2 Cr^{3+} ions per surface unit cell one derives an individual Cr^{3+} moment of 2.6×10^{-23} Am^2 $= 2.8\mu_B$ when taking into account an area of 63.9×10^{-20} m^2 of the hexagonal 1×1 surface mesh. This experimental value of the Cr^{3+} magnetic moment is in reasonable agreement with first principles theoretical prediction as well as a basic estimate from Hund's rule. The latter predicts a Cr^{3+} moment of $3\mu_B$ for the $J = S = 3/2$ total angular momentum of the 3d electrons with quenched orbital momentum and Landé-factor g = 2. Note that in Cr_2O_3 (0001) thin films moderate axial magnetic cooling fields are sufficient to favor the FM (0001) surface order without the necessity for magnetoelectric annealing. This indicates that the growth of AF domains stabilizing the surface magnetism starts at the surface. Here symmetry is broken and the spins get easily aligned in an applied field due to the reduced number of AF coupling nearest neighbors. The aligned surface moments act like seeds for the growth of the AF long range order through inhomogeneous nucleation.

The inset (b) of supplementary Fig. 2 shows the magnetic hysteresis loops of Cr_2O_3 (0001)/CoPd and Al_2O_3 (0001)/CoPd measured by polar Kerr magnetometry at T= 296 K after field cooling from $T > T_N$ in an axial field of $\mu_0 H$ = 0.3 T. The hysteresis of the Cr_2O_3 (0001)/Pd0.5nm/(Co0.6nmPd1.0nm)$_3$ sample (circles) shows a pronounced exchange bias loop shift of $\mu_0 H_{EB}$ =-16.7 mT (see arrow in inset (b) supplementary Fig. 2) which is absent in the hysteresis of the unpinned reference sample (triangles). Remarkably, and in contrast to regular exchange bias systems, comparison of the coercivity of both loops reveals absence of loop broadening typically associated with the exchange bias effect. This behavior reflects the unusual FM order of the Cr_2O_3 (0001) interface magnetization. The uniform FM surface state eliminates the presence of loosely coupled spins of the AF pinning layer which conventionally represent the overwhelming

DOI: 10.1038/NMAT2785

majority of AF interface spins. It is their susceptibility which is known to create loop broadening in regular exchange bias systems [50]. Similarly the exchange bias training effect is absent in Cr_2O_3 (0001)/Pd0.5nm/(Co0.6nmPd1.0nm)$_3$. Likewise, this is in accordance with the formation of a uniform FM interface state which remains stationary during the magnetization reversal of the CoPd top layer. The invariant interface magnetization suppresses spin configurational changes in the AF pinning layer. In regular AF/FM heterostructures these spin configurational changes are responsible for the gradual decay of the exchange bias field with consecutively cycled hysteresis loops [51].

Supplementary Fig. 3 shows the temperature dependence of the exchange bias field, $\mu_0 H_{EB}$ vs. T, measured after magnetic field cooling (circles) and magnetoelectric annealing in $E = \pm$ 1.62 kV/mm electric and $\mu_0 H$ = 0.3 T magnetic field (diamonds E<0, triangles E>0) for increasing temperature, respectively. Magnetic field cooling in E=0 creates regular exchange bias. Magnetoelectric annealing in negative electric and positive magnetic field, EH<0, gives rise negative exchange bias fields. The positive field product EH>0 gives rise to positive exchange bias in agreement with the recently observed thermally induced magnetoelectric switching in Cr_2O_3 (0001)/CoPt reported in (Ref. 13). The complete temperature dependence of $\mu_0 H_{EB}$ vs. T presented here for Cr_2O_3 (0001)/CoPd reveals the nature of a unique exchange bias phenomenon and its relation to the FM state of the Cr_2O_3 (0001) surface. Most striking is the steep onset of the exchange bias field in $\mu_0 H_{EB}$ vs. T at $T < T_N$. This unusual T-dependence is a fingerprint of the order-parameter type temperature behavior of the interface magnetization. It is in accordance with the Meiklejohn Bean description of exchange bias,

$$\mu_0 H_{EB} = -\frac{J S_{Cr_2O_3} S_{CoPd} Cos\theta}{M_{CoPd} t_{CoPd}},$$

when applied to the specific FM interface magnetization. The exchange bias field is proportional to $S_{Cr_2O_3}$. Hence, $\mu_0 H_{EB}$ is expected to resemble characteristics of the temperature dependence of $S_{Cr_2O_3}$. In fact, the single parameter fit $\mu_0 H_{EB} = const.\sqrt{T_N - T}$ represented by the red line in the supplementary Fig. 3 describes the $\mu_0 H_{EB}$ vs. T data for 290K<T<307K obtained after magnetic field cooling in E = 0. The classical power law behavior expresses both the T-dependence of the exchange bias field (supplementary Fig. 3 red line) and the temperature dependence of the Kerr signal of the Cr_2O_3 (0001) film (compare red line in supplementary Fig. 2) following $S_{Cr_2O_3}(T)$, respectively.

A second remarkable and rather unusual feature is the saturation of $\mu_0 H_{EB}$ with decreasing temperature followed by a prominent decrease of $\mu_0 H_{EB}$ vs. T which sets in at $T \approx 210$ K. This decrease in the exchange bias field appears to be accompanied by a change in the magnetism of the Cr_2O_3 (0001) surface which we tentatively associate with a temperature dependent tilting of the magnetization at the interface in the exchange bias heterostructure. A number of experimental findings point in this direction. First, our own photoemission data measured at T = 100K require some amount of tilting to produce detectable intensity. Second, the temperature dependence of the normal component of the magnetization of the Cr_2O_3 (0001) film displayed in the inset (a) of supplementary Fig. 2 shows a decrease which is likely the result of tilting of the Cr surface spins. Finally there are recent studies on Cr_2O_3 (0001)-based exchange bias systems using FM thin films with

in-plane magnetic anisotropy. In accordance with the phenomenological Meiklejohn Bean description above orthogonal orientation of the FM and AF interface magnetization with $\theta = \pi/2$ gives rise to $Cos\theta = \mu_0 H_{EB} = 0$. In fact systems such as Cr_2O_3 (0001)\Fe and Cr_2O_3 (0001)\Co show zero or virtually zero exchange bias at temperatures $T^* < 210K < T < T_N$ with system dependent T^* [52,53]. Below T^* in-plane exchange bias sets in accordance with a temperature driven tilting of the Cr interface spins allowing for non zero $Cos\theta$.

4. Supplementary Movie Legend

The movie is based on a cartoon of our Cr_2O_3 (0001)/Pd0.5nm/(Co0.6nmPd1.0nm)$_3$ heterostructure. The Cr_2O_3 atomic and spin structure is represented in accordance with Fig. 1 and supplementary Fig. 1. The CoPd ferromagnetic thin film is represented by a simplified spin structure using localized spins despite the fact that CoPd is an itinerant ferromagnet. Electric fields are "measured" by a multimeter and applied via electrodes (dark yellow films) sandwiching the heterostructure. The applied voltages are displayed on the multimeter. While the movie progresses the voltages change from 0 to +1.5kV then back to -1.7kV. A small constant magnetic field is applied in the direction indicated by the blue arrow simultaneously with the applied electric fields. The magnetic hysteresis, M/M_s *vs.* $\mu_0 H$, of the CoPd film is shown after exposure of each individual field-product. Clearly the switching of the AF domain state and the exchange bias field can be seen at $\approx \pm 1.4$kV (note that all the numerical values used in this movie do not precisely follow the experimental data). In addition to the pronounced switching effect we show largely exaggerated the electrically controlled exchange bias due to the linear magnetoelectric effect of Cr_2O_3.

5. Supplementary Notes

37. Vescovo E., et al., U5UA: A new high-resolution undulator beamline at the NSLS for spin-resolved photoemission speptroscopy, *Synch. Rad. News* **12** 10 (1999).
38. Johnson P.D., et al., Spin-polarized photoemission spectroscopy of magnetic surfaces using undulator radiation, *Rev. Sci. Instrum.* **63** 1902 (1992).
39. Johnson P.D., Potassium Adsorption and an Unoccupied Surface State on Fe(001), *Rep. Prog. Phys*. **60** 1217 (1997).
40. Blöchl P.E., Projector augmented-wave method, *Phys. Rev. B* **50**, 17953 (1994).
41. Kresse G. and Furthmüller J., Efficient iterative schemes for *ab initio* total-energy calculations using a plane-wave basis set, *Phys. Rev. B* **54**, 11169 (1996).
42. Kresse G. and Joubert D., From ultrasoft pseudopotentials to the projector augmented-wave method, *Phys. Rev. B* **59**, 1758 (1999).
43. Kresse G. & Furthmüller J., Efficiency of ab-inito energy calculations for metals and semiconductors using a plane-wave basis set, *Comput. Mater. Sci.* **6**, 15-50 (1996).
44. Kresse G. & Hafner J., Ab initio molecular dynamics for open-shell transition metals, *Phys. Rev. B*, **48**, 13115-13118 (1993).
45. Liechtenstein A. I., Anisimov V. I., and Zaanen J., Density-functional theory and strong interactions: Orbital ordering in Mott-Hubbard insulators, *Phys. Rev. B* **52**, R5467 (1995).

DOI: 10.1038/NMAT2785

46. Shi S.-Q., Wysocki A. L., and Belashchenko K. D., Magnetism of Chromia from First-Principles Calculations, *Phys. Rev. B* **79**, 104404 (2009).
47. Monkhorst H. and Pack J. D., Special points for Brillouin-zone integrations, *Phys. Rev. B* **13**, 5188 (1976).
48. Blöchl P. E., Jepsen O., and Andersen O. K., Improved tetrahedron method for Brillouin-zone integrations, *Phys. Rev. B* **49**, 16223 (1994).
49. Krichevtsov B. B., Pavlov V. V., Pisarev R. V., and Gridnev V. N., Spontaneous non-reciprocal reflection of light from antiferromagnetic Cr_2O_3, *J. Phys. Condens. Mat.* **5**, 8233 (1993).
50. Scholten G., Usadel K. D., and Nowak U., Coercivity and exchange bias of ferromagnetic/antiferromagnetic multilayers, *Phys. Rev. B* **71**, 064413 (2005).
51. Binek Ch., Training of the exchange-bias effect: A simple analytic approach, *Phys. Rev. B*. **70**, 014421 (2004).
52. Sahoo S., Mukherjee T., Belashchenko K. D., and Binek Ch., Isothermal low-field tuning of exchange bias in epitaxial Fe/Cr_2O_3/Fe. *Appl. Phys. Lett*. **91**, 172506 (2007).
53. Shiratsuchi Yu, Nakatani T., Kawahara S. I., and Nakatani R., Magnetic coupling at interface of ultrathin Co film and antiferromagnetic Cr_2O_3(0001) film. *J. of Appl. Phys*. **106**, 033903 (2009).